



MOL2NET, International Conference Series on Multidisciplinary Sciences
USEDAT-08: USA-Europe Data Analysis Training Program Workshop,
UPV/EHU, Bilbao-MDC, Miami, USA, 2020

Ship Detection from RISAT-1 and Radarsat-2 SAR Images using CFAR

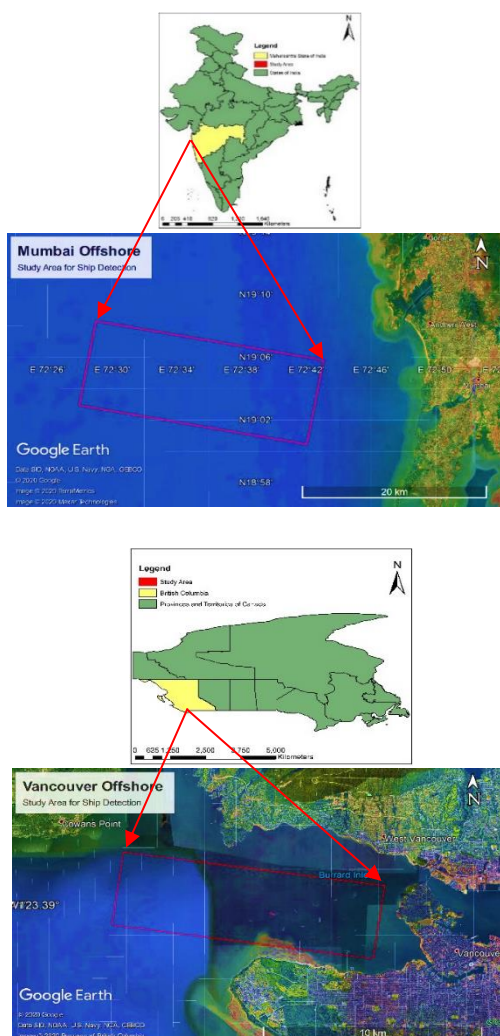
Ojasvi Saini^a *, Ashutosh Bhardwaj^a, R. S. Chatterjee^b

^a Photogrammetry and Remote Sensing Department, Indian Institute of Remote Sensing, 4, Kalidas Road, Dehradun-248001; ojasvi@iirs.gov.in, ojasvi21nov@gmail.com

^b Geoscience Department, Indian Institute of Remote Sensing, 4-Kalidas Road, Dehradun- 248001; rschatterjee@iirs.gov.in

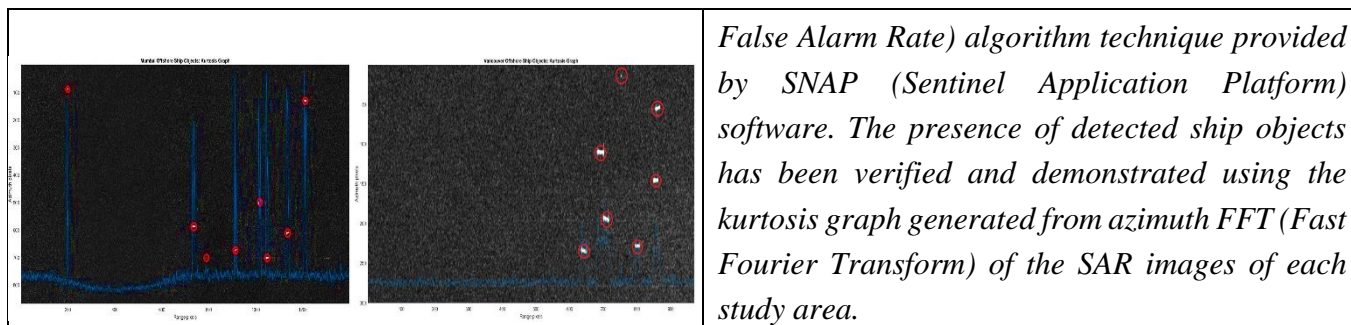
* Correspondence: ojasvi@iirs.gov.in, ojasvi21nov@gmail.com; Tel.: +91-9416556074

Graphical Abstract



Abstract.

Maritime surveillance has been an essential requirement since ancient times. However, in the absence of technology, it could not be done so effectively at that time as is being done in today's era of science and technology. The advancement in remote sensing technology has made maritime surveillance quicker and more precise. Ship detection and identification are playing a crucial role in the field of maritime surveillance in dealing with sea border activity, illegal fishery, maritime traffic, illegal migration of humans, navy movements or oil spill detection, and monitoring. The information provided by imaging radar is fundamentally different from sensors that operate in infrared and visible portions of the electromagnetic spectrum. SAR images are found to be very much suitable for the identification of sea objects because of the very bright appearance of sea objects in SAR images against dark sea surface in the background. In this present study, RISAT-1 SAR image of Mumbai offshore region (acquired on September 15, 2016) and Radarsat-2 SGF W2 mode of Vancouver, Canada (acquired on August 14, 2008) has been used for the rapid detection of ship objects using CFAR (Constant



Introduction

Being capable of accessing and monitoring the earth's surface globally with different types of sensors, remote sensing technology has become one of the most advantageous techniques as it plays a crucial role in the field of coastal and sea area monitoring and surveillance [1][2]. Synthetic Aperture Radar (SAR) is suitable for observations of the Earth's surface from space for both day and night as well as all weather conditions[3][4][5][6]. SAR emits periodic pulses of microwave signals towards the earth and records the backscattered signals coming from the targets present on the earth's surface[7]. SAR images are found to be very much suitable for the identification of sea objects because of the very bright appearance of sea objects in SAR images against dark sea surface in the background [8][9][10]. RISAT-1 is a part of the satellite imaging mission of ISRO (Indian Space Research Organization) operating with a C-band SAR active radar imager[11] and Radarsat-2 is a satellite mission of CSA (Canadian Space Agency) operating with C-band SAR active radar imager[12]. In this present study, RISAT-1 SAR image of the Mumbai offshore region and Radarsat-2 SGF W2 mode of Vancouver, Canada has been used for the rapid detection of ship objects using the European Space Agency's (ESA) SNAP software's tool consisting of the CFAR algorithm. The tool is called "ocean object detection" and allows rapid ship detection mapping. Along with the detection of sea objects (ships) the presence of detected ship objects has also been verified and demonstrated using kurtosis graph generated from the one dimensional FFT in Azimuth direction.

Materials and Study Area

In the present study, the subsets RISAT-1 dual polarimetric (HH, HV) SAR image of the Mumbai offshore region (acquired on September 15, 2016) and Radarsat-2 dual polarimetric SGF W2 mode SAR image of Vancouver, Canada (near Burrard inlet) acquired on August 14, 2008) have been used. The HV band of both the SAR images of each study area is used for the detection of ships as sea objects. The location of both the study regions and the data properties of the SAR images used are shown in figure 1 and table 1 respectively.

Table 1: Data properties for Risat-1 and Radarsat-2 dataset used in the study.

Data Properties	RISAT-1	Radarsat-2
Product ID	202828721	PDS_05117090
Date of pass	15-SEP-2016	14-AUG-2008
Product type	L1-GROUND-RANGE	SGF
Image format	GeoTIFF	GeoTIFF
Ellipsoid	WGS84	WGS 84
PASS	Descending	Ascending
Sensor orientation	Left	Right
SAR mode	Dual-Pol (HH HV)	Dual-Pol (HH HV)

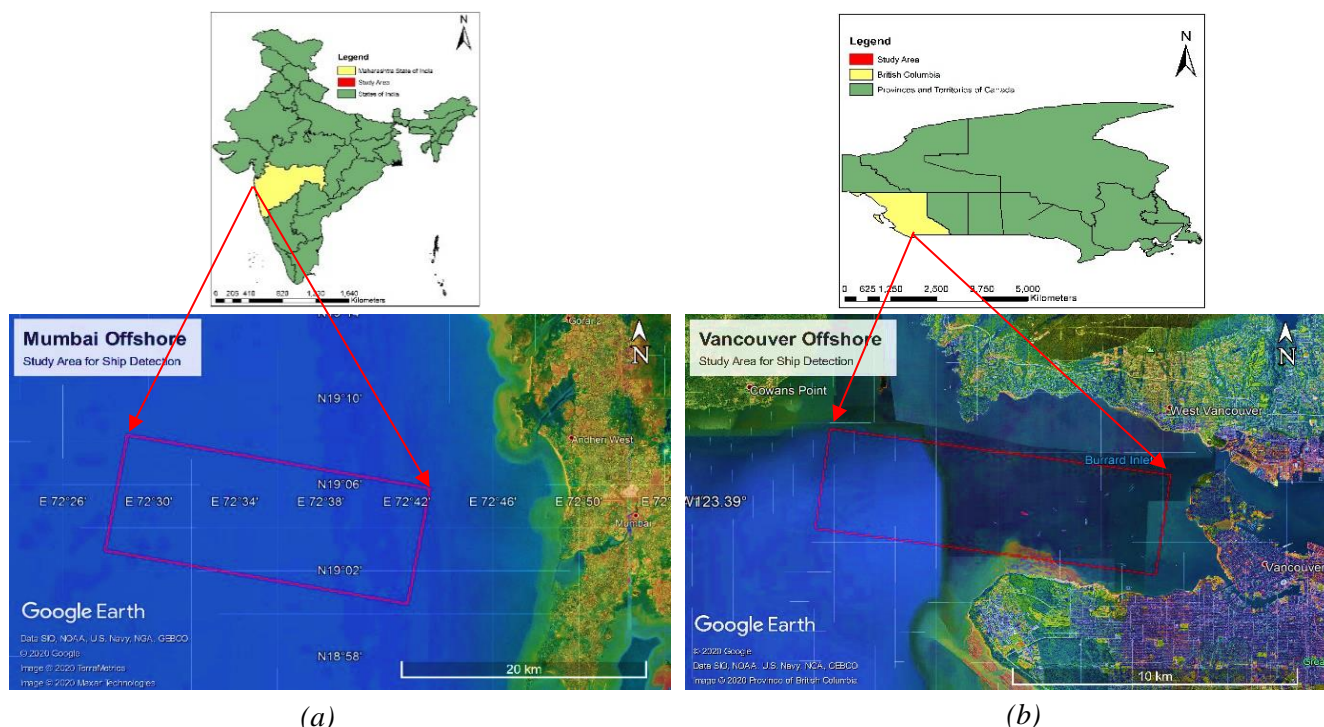


Figure 1: Geographic Locations of the footprints of subsets of the SAR images used for the study regions of Mumbai offshore (a) and Vancouver offshore (b).

Methods

The object detection operation consists of the four major operations namely Pre-processing, Land-sea masking, Pre-screening, and discrimination. The pre-processing steps includes calibration of SAR images to make the pre-screening process easier and more accurate. A land-sea masking is applied using DEM data (auto-downloadable) required for the study area to keep the detection focused only on the sea area. After this process, objects are detected with a Constant False Alarm Rate (CFAR) detector. False alarms are rejected based on the object dimension[13].

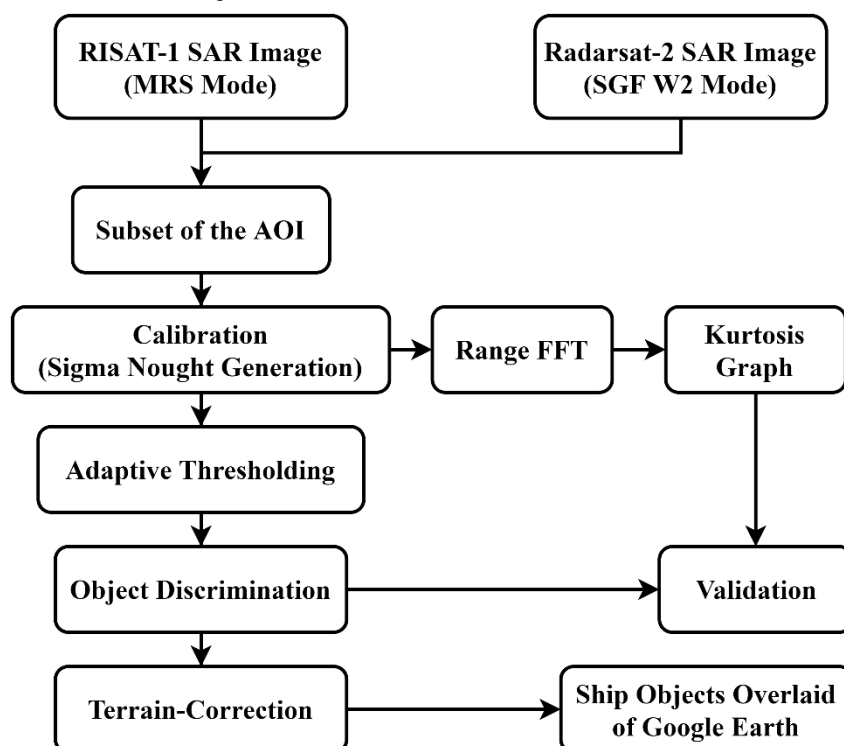


Figure 2: Flow chart for methodology used in the study.

Two-Parameter Constant False Alarm Rate (CFAR) Detector

The pre-screening operation the two-parameter constant false alarm rate (CFAR) detector is used. The key idea is to search remarkably bright pixels when compared to pixels in the neighboring area.

Let x_t be the pixel under test and T be a given threshold, then the detection criterion can be expressed as

$$x_t > T \quad \Leftrightarrow \quad \text{TARGET} \quad (1)$$

Let $f(x)$ be the ocean clutter probability density function and x range through the possible pixel values, then the probability of false alarm (PFA) is given by

$$\text{PFA} = \int_T^{\infty} f(x) dx \quad (2)$$

and the above detection criterion is equivalent to the criterion below

$$\int_{x_t}^{\infty} f(x) dx < \text{PFA} \quad \Leftrightarrow \quad \text{TARGET} \quad (3)$$

If Gaussian distribution is assumed for the ocean clutter, the above detection criterion can be further expressed as

$$x_t > \mu_b + \sigma_b t \quad \Leftrightarrow \quad \text{TARGET} \quad (4)$$

where μ_b is the background mean, σ_b is the background standard deviation and t is a detector design parameter which is computed from PFA by the following equation

$$\text{PFA} = \frac{1}{2} - \frac{1}{2} \text{erf}\left(\frac{t}{\sqrt{2}}\right) \quad (5)$$

The valid range of PFA value is $[0, 1]$. A setup shown in Figure 3 is used In the execution of the two-parameter CFAR detector. The target window holds the pixel under test, the background “ring” contains pixels for estimating the underlying background statistics. So that no pixels of an extended target are included in the background ring, the guard “ring” separates the target window from the background ring. The used background mean μ_b and the standard deviation σ_b in the criterion are estimated from the pixels in the background ring.

In case that the target window contains more than one pixel, this operator uses the following detection criterion

$$\mu_t > \mu_b + \sigma_b t \quad \Leftrightarrow \quad \text{TARGET} \quad (6)$$

Where μ_t is the mean value of pixels in the target window. In this case, t should be replaced by $t\sqrt{n}$ (where n is the number of pixels in the target window) in the PFA calculation.

Adaptive Threshold Algorithm

An adaptive approach is used for the object detection with the help of Adaptive Thresholding operator. There are three windows as shown in figure 3, for each pixel under test, namely the target window, guard window, and background window. Normally, the size of the target window should be comparable with the size of smallest object to detect (50 m in this study), the size of guard window (500 m in this study) and the largest object to detect should be comparable, and the background window size (800 m in this study) should be large enough to estimate accurately the local statistics. The operator first computes the detector design parameter t from user-selected PFA using the equation above. Then computes

background mean μ_b and standard deviation σ_b using pixels in the background ring. Next, compute the mean value μ_t of the target window. If $\mu_t > \mu_b + \sigma_b$, then the center pixel is detected as part of an object, otherwise not an object. Then the algorithm moves all windows by one pixel to detect the next pixel.

Discrimination

The Object Discrimination operator conducts the discrimination operation. Based on simple target measurements, false detections are eliminated during this operation. First, the contiguous detected pixels are clustered into a single cluster with the operator. Then the width and length information of the clusters are extracted. Finally, clusters that are too big or too small are eliminated based on these measurements and user input discrimination criteria.

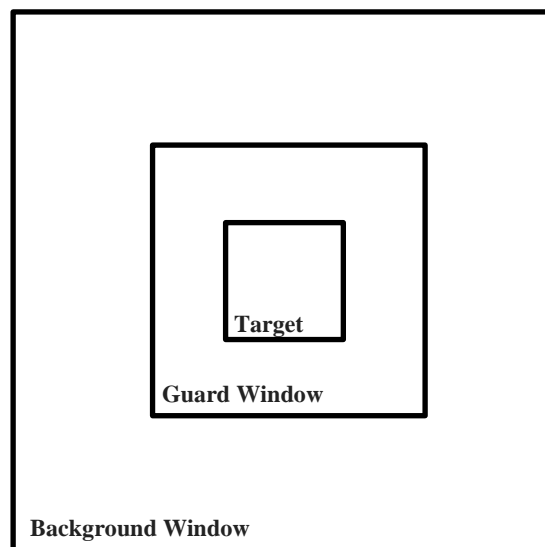


Figure 3: Window setup for adaptive threshold algorithm.

Validation of the results using Azimuth FFT and Kurtosis Graph

In the dark background of the sea surface, the presence of the bright ship targets is interpretable in the kurtosis graph generated using azimuth FFT algorithm applied to subsetting SAR image of the study area as shown in figure 5 and 7. The peaks of the kurtosis graph are overlaying on the same range columns which are containing the bright ship objects.

Results and Discussion

For the subsets of the RISAT-1 SAR image of the Mumbai offshore region and Radarsat-2 SAR image for the Vancouver ocean region total of eight and seven ship targets respectively were detected using the algorithm. Geographic locations of detected ship objects with their lengths, breadths, and pixel indices for the Mumbai offshore study area as well as Vancouver Ocean are shown in table 2 and table 3. Detected ship objects are overlaid on Google Earth imagery and represented by small white circles as shown in figure 4 and figure 6. The verification of the detected ship target objects can also be observed with the kurtosis graph of Azimuth FFT of the SAR images of the study areas as shown in figure 5. In the dark background of the sea surface, the presence of the bright ship targets is interpretable in the kurtosis graph generated using azimuth FFT algorithm applied to subsetting SAR image of the study area as shown in figure 5 and 7. The peaks of the kurtosis graph are overlaying on the same range columns which are containing the bright ship objects. Only those ship objects detected by the CFAR algorithm

could not be represented by the kurtosis peaks, which were very much faint in the unprocessed SAR image as shown in Figures 5 and 7.

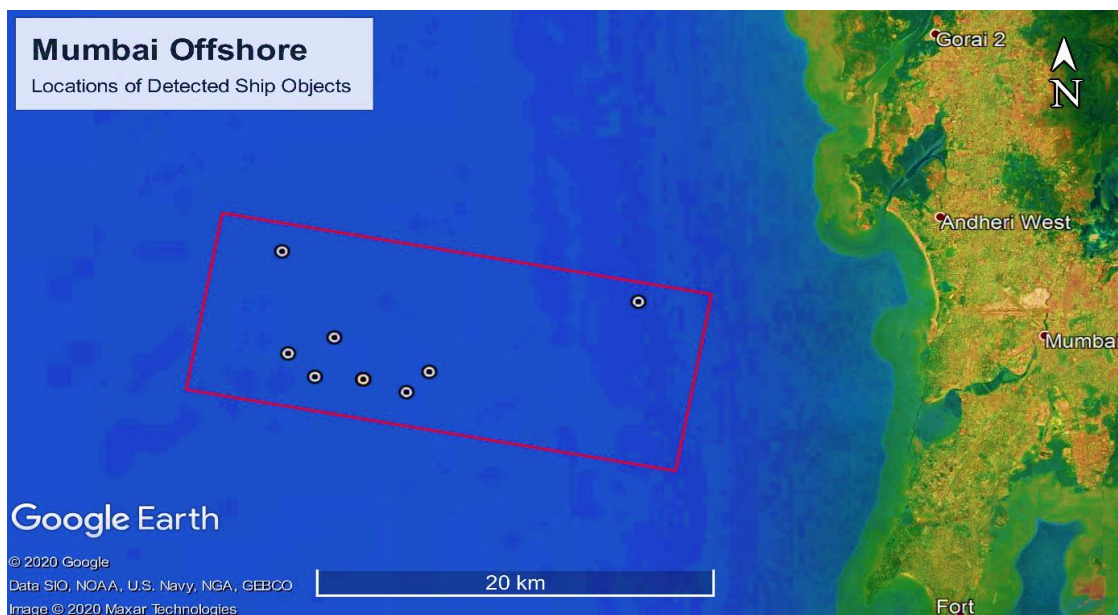


Figure 4: Detected ship objects overlaid on Google Earth imagery for Mumbai offshore study area

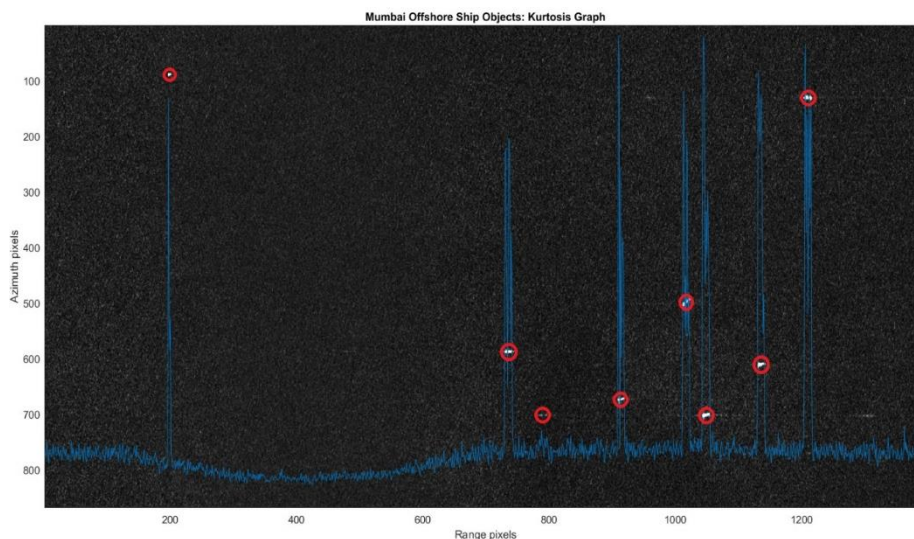


Figure 5: Demonstration of detected ship objects for Mumbai offshore study area using kurtosis graph

Table 2: Geographic locations of detected ship objects with their lengths, breadths and pixel indices for Mumbai offshore study area.

Detections	x	y	Latitude	Longitude	Width	Length
target_00	5287	4028	19.0938895	72.6834813	162	104.67
target_01	6299	4070	19.1194175	72.5127709	306	151.19
target_02	5824	4526	19.0583261	72.5833236	288	93.04
target_03	6002	4614	19.054553	72.5517123	252	151.19
target_00	6106	4438	19.0757623	72.5378463	270	197.71
target_05	6224	4550	19.0676546	72.5157237	288	139.56
target_00	6003	4614	19.0545677	72.5516284	270	151.19
target_00	6137	4640	19.0558034	72.5285327	288	139.56

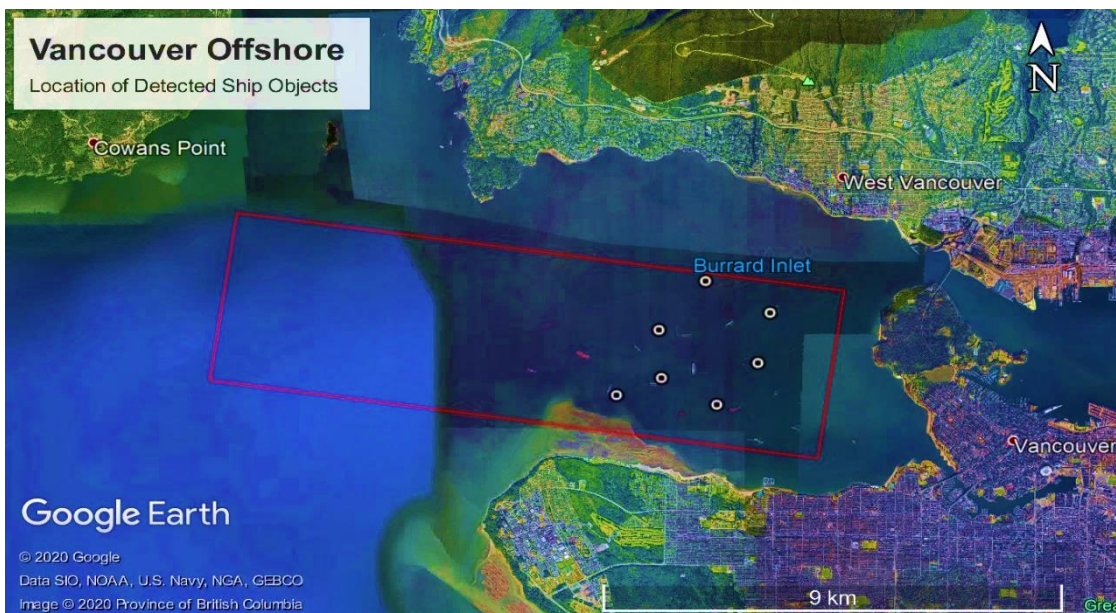


Figure 5: Detected ship objects overlaid on Google Earth imagery for Vancouver offshore study area

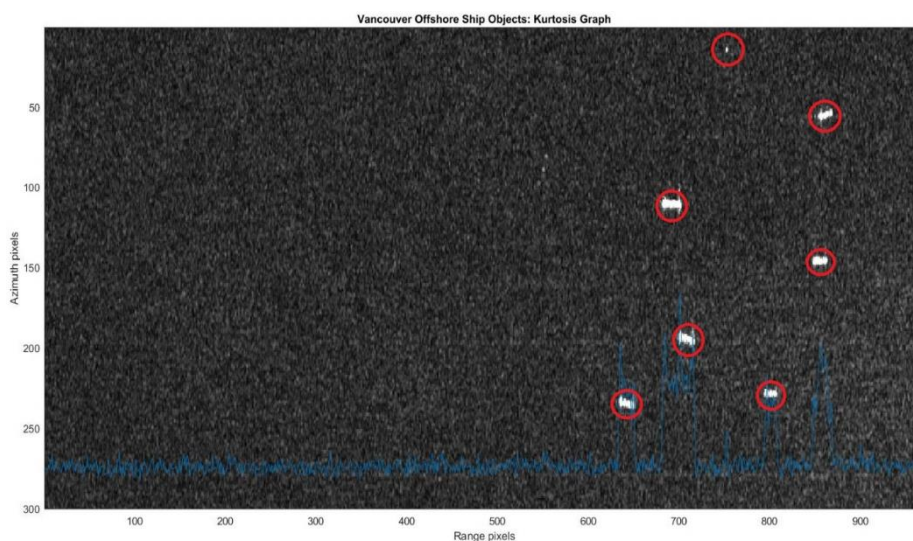


Figure 4: Demonstration of detected ship objects for Vancouver offshore study area using kurtosis graph.

Table 3: Geographic locations of detected ship objects with their lengths, breadths, and pixel indices for Vancouver offshore study area.

Detections	x	y	latitude	Longitude	Width	Length
target_000	3641	4470	49.31454	-123.204	50	50
target_001	3750	4511	49.30823	-123.186	225	125
target_002	3581	4566	49.30483	-123.216	287.5	125
target_003	3744	4602	49.29827	-123.189	237.5	112.5
target_004	3597	4650	49.29529	-123.216	262.5	137.5
target_005	3690	4684	49.29002	-123.201	212.5	112.5
target_006	3531	4690	49.2919	-123.228	262.5	137.5

Conclusions

The study concludes that although CFAR is a very popular technique for vessel detection using SAR images, the kurtosis graphs generated from range and azimuth FFT land-masked SAR images can be used for the preliminary knowledge of the presence of ship objects in the ocean. In the dark background of the sea surface, the presence of the bright ship targets is easily interpretable in the kurtosis graph generated using azimuth FFT algorithm applied to subsetting SAR image of the study areas as shown in figure 5 and 7. The peaks of the kurtosis graph are overlaying on the same range columns which are containing the bright ship objects.

References

- [1] S. K. Chaturvedi, "Study of synthetic aperture radar and automatic identification system for ship target detection," *J. Ocean Eng. Sci.*, vol. 4, no. 2, pp. 173–182, 2019.
- [2] M. F. Bruno *et al.*, "A combined approach of field data and earth observation for coastal risk assessment," *Sensors (Switzerland)*, vol. 19, no. 6, pp. 1–20, 2019.
- [3] Z. Pan, L. Liu, X. Qiu, and B. Lei, "Fast vessel detection in gaofen-3 SAR images with ultrafine strip-map mode," *Sensors (Switzerland)*, vol. 17, no. 7, pp. 1–19, 2017.
- [4] Q. An, Z. Pan, and H. You, "Ship detection in gaofen-3 SAR images based on sea clutter distribution analysis and deep convolutional neural network," *Sensors (Switzerland)*, vol. 18, no. 2, 2018.
- [5] S. Wang, M. Wang, S. Yang, and L. Jiao, "New Hierarchical Saliency Filtering for Fast Ship Detection in High-Resolution SAR Images," *IEEE Trans. Geosci. Remote Sens.*, vol. 55, no. 1, pp. 351–362, 2017.
- [6] P. Iervolino and R. Guida, "A Novel Ship Detector Based on the Generalized-Likelihood Ratio Test for SAR Imagery," *IEEE J. Sel. Top. Appl. Earth Obs. Remote Sens.*, vol. 10, no. 8, pp. 3616–3630, 2017.
- [7] C. Oliver and S. Quegan, *Understanding synthetic aperture radar images(Book)*. 1997.
- [8] U. Kanjir, H. Greidanus, and K. Oštir, "Vessel detection and classification from spaceborne optical images: A literature survey," *Remote Sens. Environ.*, vol. 207, no. November 2016, pp. 1–26, 2018.
- [9] A. Marino, M. J. Sanjuan-Ferrer, I. Hajnsek, and K. Ouchi, "Ship detection with spectral analysis of synthetic aperture radar: A comparison of new and well-known algorithms," *Remote Sens.*, vol. 7, no. 5, pp. 5416–5439, 2015.
- [10] M. Amoon, A. Bozorgi, and G. Rezai-rad, "New method for ship detection in synthetic aperture radar imagery based on the human visual attention system," *J. Appl. Remote Sens.*, vol. 7, no. 1, p. 071599, 2013.
- [11] T. Misra *et al.*, "Synthetic Aperture Radar payload on-board RISAT-1: Configuration, technology and performance," *Curr. Sci.*, vol. 104, pp. 446–461, 2013.
- [12] C. Livingstone, I. Sikaneta, and C. Gierull, "RADARSAT-2 system and mode description," *Def. Res. Dev. Canada Ottawa*, no. 2005, pp. 1–22, 2006.
- [13] D. J. Crisp, "The State-of-the-Art in Ship Detection in Synthetic Aperture Radar Imagery," *Inf. Sci. (Ny)*, no. DSTO-RR-0272, p. 115, 2004.